CLASSIFICATION: BIOLOGICAL SCIENCES, Immunology and Inflammation

TITLE: Endothelial Wnt/β-catenin signaling reduces immune cell infiltration in multiple sclerosis

AUTHORS: Justin E. Lengfeld[1,7], Sarah E. Lutz[2,7,*], Julian R. Smith[2], Claudiu Diaconu[2], Cameron Scott[1], Sigal B. Kofman[3], Claire Choi[2], Craig M. Walsh[4], Cedric S. Raine[5], Ilir Agalliu[6], and Dritan Agalliu[1,2,*]

AUTHOR AFFILIATIONS:

1. Department of Developmental and Cell Biology, University of California, Irvine CA 92697, USA.

2. Departments of Neurology, Pathology & Cell Biology and Pharmacology, Columbia University Medical Center, New York, NY 10032, USA.

3. Department of Medicine, Columbia University Medical Center, New York, NY 10032, USA.

4. Department of Molecular Biology and Biochemistry, University of California, Irvine CA 92697, USA.

5. Department of Pathology, Albert Einstein College of Medicine, Bronx, NY 10461, USA.

6. Department of Epidemiology and Population Health, Albert Einstein College of Medicine, Bronx, NY 10461, USA.

7. Equal contribution

*Corresponding authors; D.A.: E-mail: da191@cumc.columbia.edu; Phone: 212-305-0323. S.E.L: E-mail: sl4151@cumc.columbia.edu.

SUPPLEMENTARY INFORMATION

SUPPLEMENTARY MATERIALS AND METHODS

Mice: All experimental procedures were approved by the IACUC/IRB committees at the University of California, Irvine and Columbia University Medical Center. Wild-type C57BL/6J, TCF/LEF::H2B-eGFP reporter (1), VE-Cadherin::tTA (2) and TRE-Axin-IRES-eGFP (3) strains were purchased from the Jackson Laboratory. The TCF/LEF::H2B-eGFP strain expresses a H2B-eGFP fusion protein under the control of six copies of the *TCF/LEF1* response element (Fig. 1A). This transgene was backcrossed for 10 generations to C57BL/6J mice to produce a congenic strain, prior to induction of EAE. Wnt/β-catenin pathway loss-of-function mice were produced by crossing the VE-Cadherin::tTA (2) with TRE-Axin-IRES-eGFP strains (3). Both lines were backcrossed for at least 8 generations to C57BL6/J animals prior to EAE induction. Pregnant dams carrying either doubly transgenic (dTg) or singly transgenic (sTg) control pups were fed during gestation with 2020 chow supplemented by 625 mg/kg doxycyline (Harlan), to suppress transgene expression and allow normal function of the Wnt/β-catenin pathway during development. At birth, the doxycycline chow was replaced by a regular diet, allowing the Tet_{OFF} system to induce expression of Axin and eGFP in dTg mice (Fig. 4A and 5A).

Experimental autoimmune encephalomyelitis induction: EAE was induced in 10- to 12-week-old female mice by subcutaneous injections with 100 μl of emulsion containing 100 μg of the myelin oligodendrocyte glycoprotein peptide MOG_{35-55} (MEVGWYRSPFSRVVHLYRNGK; ThermoFisher Scientific) in PBS, with complete Freund's adjuvant (CFA) containing 200 μg *Mycobacterium tuberculosis* H37Ra (DIFCO Laboratories). The day of MOG immunization was designated as day 0. Mice received intravenous injections with 400 ng of *Bordetella pertussis* toxin (List Biological Laboratories, Campbell, CA) 0 and 2 days post-immunization (dpi). Control animals received an emulsion containing PBS/CFA and *B. pertussis* toxin without MOG. Mice were examined for clinical

signs of EAE using the following scale with 0.5-point gradations for intermediate presentation: 0, no signs; 1, completely flaccid tail; 2, hind limb paresis; 3, hind limb paralysis; 4, hind limb and forelimb paralysis; 5, moribund (4, 5). The disease was monophasic, with an onset at 8-10 dpi and peak clinical score at 12-16 dpi. Control animals sensitized with PBS/CFA emulsion and *B. pertussis* toxin did not exhibit any clinical signs.

Patient samples and immunohistochemistry: Patient tissues were provided by Dr. C. S. R (Albert Einstein College of Medicine; IRB protocol #89-31) and the Human Brain and Spinal Fluid Resource Center, VA West Los Angeles Healthcare Center, Los Angeles, CA90073, which is sponsored by NINDS/NIMH, NMSS and Department of Veterans Affairs (D.A.; IRB protocol #AAAQ7343). Paraffin-embedded brain tissues from 12 MS patients and 5 non-neurological disease controls (Table S2) were used to assess SOX17 expression. Fresh frozen brain tissues from 6 MS patients and 5 non-neurological disease controls (Table S2) were used to assess APCDD1 expression. Deparaffinized sections underwent antigen retrieval for 35 minutes at 100°C (Target Retrieval Solution, pH 6; Dako, Carpinteria, CA). Peroxidase activity was quenched with 3% H_2O_2 for 10 minutes. Sections were blocked with 2.5% horse serum, incubated with primary antibody for 18 h at 4°C, followed by ImmPRESS anti-mouse Ig peroxidase (Vector Labs, Burlingame, CA) and development with peroxidase-conjugated 3,3'-diaminobenzidine (Catalog # SK-4100; Vector Labs, Burlingame, CA). Washes were performed with 0.1% Tween-20 in PBS. Sections were counterstained with hematoxylin, then dehydrated and mounted with Permount. Adjacent serial sections were immunostained for SOX17 (Acris, Rockville, MD, Catalog # TA500281 at 1:25), myelin basic protein (Biolegend, San Diego, CA; Catalog # SMI-99 at 1:4000), and non-phosphorylated neurofilament heavy chain (Biolegend San Diego, CA; Catalog # SMI-32 at 1:500). Images were captured using a Nikon Eclipse Ti inverted microscope equipped with DIC optics using 4X, 10X, and 60X (NA1.4 Plan APO VC oil) objectives,

with 1X or 1.5X in-line magnification and a Digital Sight DS-Fi1 camera. MS lesions were staged as active (n=6) or chronic silent (n=6) (6). Active lesions exhibited demyelination (loss of myelin basic protein, MBP), intense perivascular infiltrate, astrocytic hypertrophy at lesion edges surrounding the hypocellular demyelinated lesion core. Chronic active lesions exhibited active inflammation at lesion edges surrounding the hypocellular demyelinated lesion core. Chronic silent lesions exhibited sharply demarcated edges of demyelination, gliosis, axonal dystrophy, and minimal perivascular infiltrates. Myelinated regions with a normal microscopic appearance at least 3 mm from the edge of a lesion were characterized as normal-appearing white matter (NAWM) (n=7). Since SOX17 is expressed and required for normal arterial specification (7), we focused on venules. SOX17 expression was characterized in all venules (lack of smooth muscle banding, 20-60um diameter) in healthy patients, NAWM, active zones and throughout chronic silent lesions of MS patients. In SOX17-stained sections, accumulation of DAB reaction product in endothelial nuclei was scored as 0=none detected, 1+=low, 2+=moderate, 3+=high. We scored vessels on the basis of their highest-expressing EC member because not all EC nuclei per vessel were visualized in each 5 μm section.

Western blot analysis: Fluorescence Western blot analysis and quantitation with the LICOR system was performed as described (8). Spinal cords were collected from mice after perfusion with phosphate-buffered saline (PBS). Human brain white matter and mouse spinal cords were homogenized in lysis buffer containing protease and phosphatase inhibitors (ThermoFisher), followed by sonication to shear genomic DNA and RNA. Protein levels in human white matter and C57BlL/6J and sTg or dTg EAE whole spinal cord lysates were assessed with the Odyssey SA infrared imaging system (LI-COR, Lincoln. NE). The following primary antibodies were used: rabbit anti APCDD1 [1:500 (9)], Cadherin-5 (1:1000, Abcam), Claudin-5 (1:2000, Invitrogen), Occludin (1:2000, Invitrogen), ZO-1 (1:1000, Invitrogen), β-catenin (1:1000, Abcam), α-catenin (1:1000, Abcam), Caveolin-1 (1:2000, Abcam),

Cavin-2 (1:1000, Abcam) and β-actin (1:10000, Abcam). IRDyes 680 and 800 (1:10000; LI-COR) were used as secondary antibodies and Odyssey imaging software was used to quantify protein levels. Quantification values displayed are protein levels corrected first using β-actin than normalized to healthy control values.

Immunofluorescence: Brains and spinal cords were harvested from wild-type C57BL/6J, TCF/LEF::H2B-eGFP Wnt reporter mice and sTg and dTg mice. Tissue was fixed for 2 h with 4% PFA in PBS, washed with PBS and cryoprotected in 30% sucrose before embedding in TissueTek, as described (8). Sections were stained with antibodies against eGFP (1:2000, Abd Serotec), Glut-1 (1:2000, Calbiochem), Caveolin-1 (1:2000; Abcam) Sox17 (1:100, R&D Systems), GFAP (1:2000, Abcam), NeuN (1:500, Millipore), CD4 (1:100, BD Pharmigen), VCAM-1 (1:100, eBioscience), ICAM-1 (1:100, eBioscience) and Fluoromyelin (1:300, Life Technologies). Images were acquired with an LSM700 confocal microscope and quantified with Fiji software.

In situ *hybridization and fluorescence* in situ *hybridization*: *In situ* hybridizations were performed as previously described (10) using DIG-labelled riboprobes for mouse *Wnt-1, -3, -3a, -4, -5a, -7a, -7b, -9a, -11b, Norrin* and *Apcdd1* and human *CLAUDIN-5* and *APCDD1*. The in situ hybridization protocol in human tissue contained a small modification that includes tissue permeabilization with 0.05% Tween-20 prior to addition of anti-DIG antibodies. Images were obtained with a Zeiss Axioimager microscope at 10X or 20X magnification. Fluorescence *in situ* hybridizations were performed with a DIG-labelled riboprobe for mouse *Apcdd1* as previously described (10), followed by immunofluorescence for cell-specific markers. Expression of *mRNA* signals in the spinal cord was designated as - = no expression, + = weak expression, ++ = intermediate expression and +++ = strong expression (Tables S1 and S3).

In vivo *biocytin-TMR, albumin-Alexa594, and fibrinogen leakage quantitation:* 15-16 days after immunization with MOG/CFA (or PBS/CFA controls), mice received intravenous injections of 1% biocytin-TMR or albumin-Alexa594 (Life Technologies). Mice were perfused with 4% paraformaldehyde/PBS 30 min after tracer injections. Spinal cords and livers were processed and sectioned as described above. Immunofluorescence was performed with antibodies against fibrinogen (1:4000, Lifespan Bio LS-C150799) or pan-laminin (1:4000, Sigma) and counterstained with DAPI. Streptavidin-Alexa594 (1:1000; Life Technologies) was used to visualize biocytin-TMR distribution. Albumin-Alexa594 was visualized without amplification. Sections were imaged with a Zeiss LSM700 confocal microscope and analyzed with Fiji software (NIH). Images were uniformly thresholded in Fiji, and areas above threshold were defined as leaky (8).

Statistical analysis: Mixed-effect ANOVA models assessing variability within subjects were used to test variances between healthy, CFA/PTX, EAE score 1, 2 and 3 mice as a fixed effect in separate models for thoracic and lumbar regions, whereas the variability in measurements within subjects (i.e. mice) were modeled as a random effect. The reference category changed from healthy, to CFAPTX, EAE score 1 or 2 for statistical comparisons. A repeated measure two-way ANOVA model using the Sidak's multiple comparison test was used to compare clinical scores over time between sTg and dTg mice with EAE. Differences in proportion of disease incidence between sTg and dTg mice with EAE were compared by Pearson's chi-squared analysis, whereas overall survival rate between sTg and dTg EAE mice was compared by Kaplan–Meier estimator survival curves and Log-Rank test. Western blots were compared between two groups with unpaired Student's t-test. Statistical analyses were performed with GraphPad Prism 6.0 Software (t-test, Mantel-Cox, repeated measures ANOVA) or STATA software (mixed effect ANOVA models and chi-squared analysis). All tests were two-sided using a significance

level α=0.05. For all statistical models and tests described above, the significance is displayed as follows: NS $p>0.05$, *$p<0.05$, **$p<0.01$, ***$p<0.001$.

SUPPLEMENTARY FIGURES AND FIGURE LEGENDS

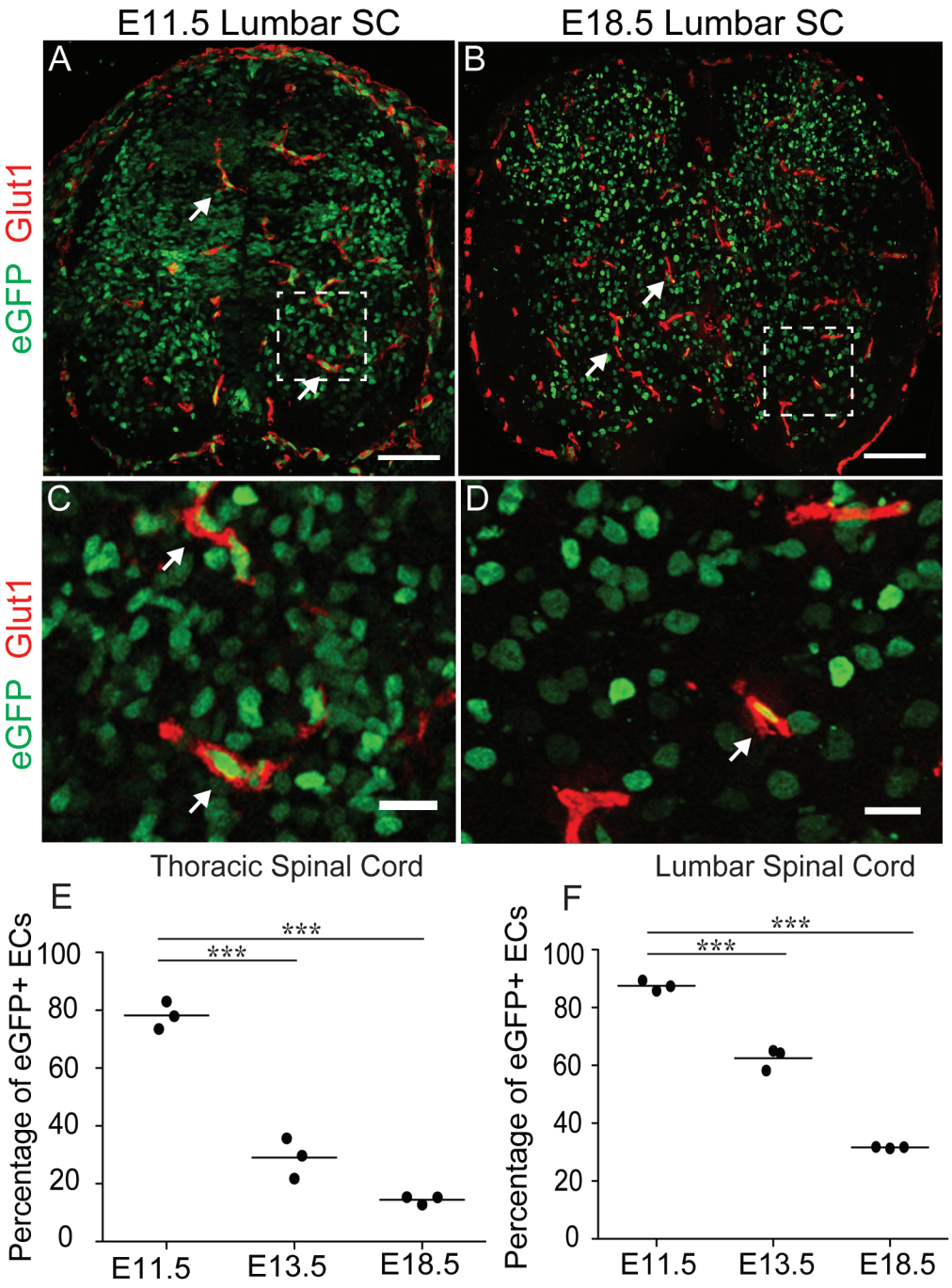

Figure S1. Embryonic expression of eGFP in CNS blood vessels of *TCF/LEF*::H2B-eGFP mouse strain. A-D) Immunofluorescence for eGFP (green) and Glut-1 (blood vessel marker, red) at e11.5 (A, C) and e18.5 (B, D) *TCF/LEF1*::H2B-eGFP (Wnt reporter) mouse lumbar neural tube. The white arrows point to eGFP^{+} EC nuclei. E, F) Dot plots of the percentage of eGFP^{+} EC nuclei in thoracic and lumbar neural tube at 3 embryonic stages. eGFP expression is significantly decreased in both thoracic and lumbar spinal cord during embryonic development (n=3 mice per group; ***p<0.001; one-way ANOVA). Scale bars (A, B) are 100 µm and (C, D) are 20 µm.

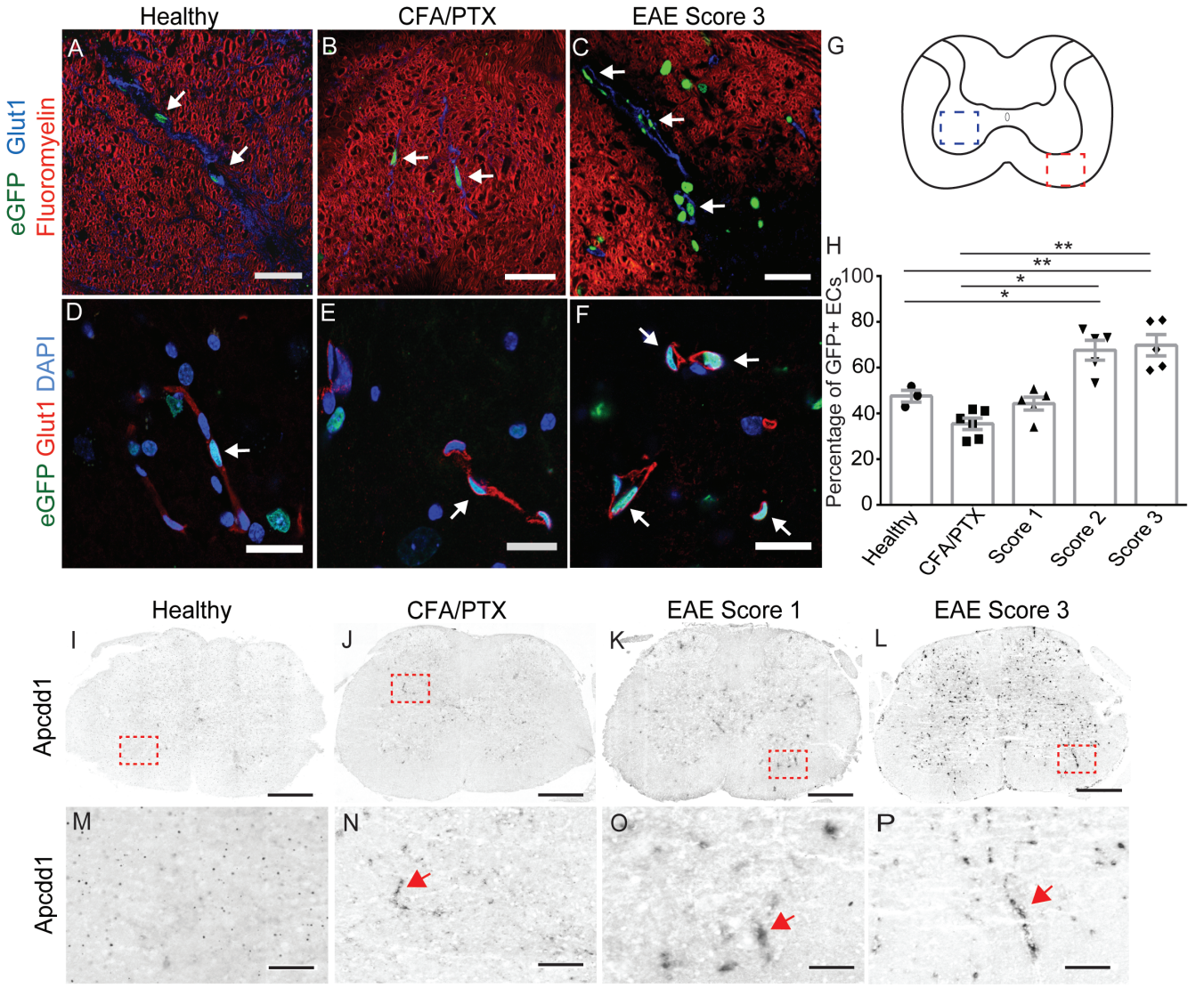

Figure S2. Wnt/β-catenin pathway is upregulated in the lumbar spinal cord ECs during EAE. (A-C) Immunofluorescence for eGFP (green), Fluoromyelin (myelin, red) and Glut-1 (blood vessels, blue) in the white matter lumbar spinal cord of *TCF/LEF1*::H2B-eGFP Wnt reporter mice. The Wnt activity (eGFP immunofluorescence) is increased in white matter ECs of the lumbar spinal cord (G, red square) during EAE. D-F) Wnt reporter activity is also increased in ECs of the gray matter lumbar spinal cord during EAE progression (G; blue square). Glut-1 (red) labels blood vessels and DAPI marks nuclei. H) Quantification of the Wnt reporter activity in lumbar spinal cord ECs during EAE progression (healthy (n=3), CFA/PTX (n=6), EAE Score 1 – 3 (n=5/score); *p<0.05, **p<0.01, ***p<0.001; mixed effect ANOVA). I-P) In situ hybridization for *Apcdd1 mRNA* during EAE progression in lumbar spinal cord. *Apccd1* mRNA expression is increased by EAE Score 1 and 3 (N-P, red arrows). Scale bar = 20 μm, except I-L (200 μm).

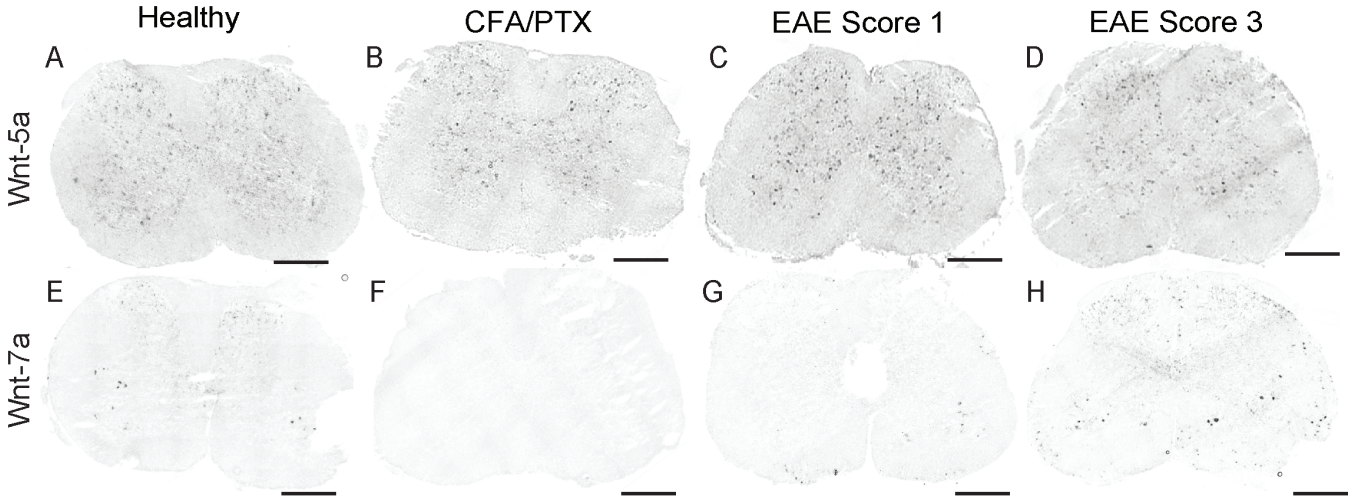

Figure S3. *Wnt-5a, but not Wnt-7a/7b* is upregulated in spinal cords during EAE progression. (A-H) *In situ* hybridization for *Wnt5a (A-D)* and *Wnt-7a (E-H)* in lumbar spinal cords from healthy, CFA/PTX controls as well as EAE scores 1 and 3 mice. *Wnt5a* mRNA is highly upregulated at EAE score 1 and 3. Scale bars are 200 μm.

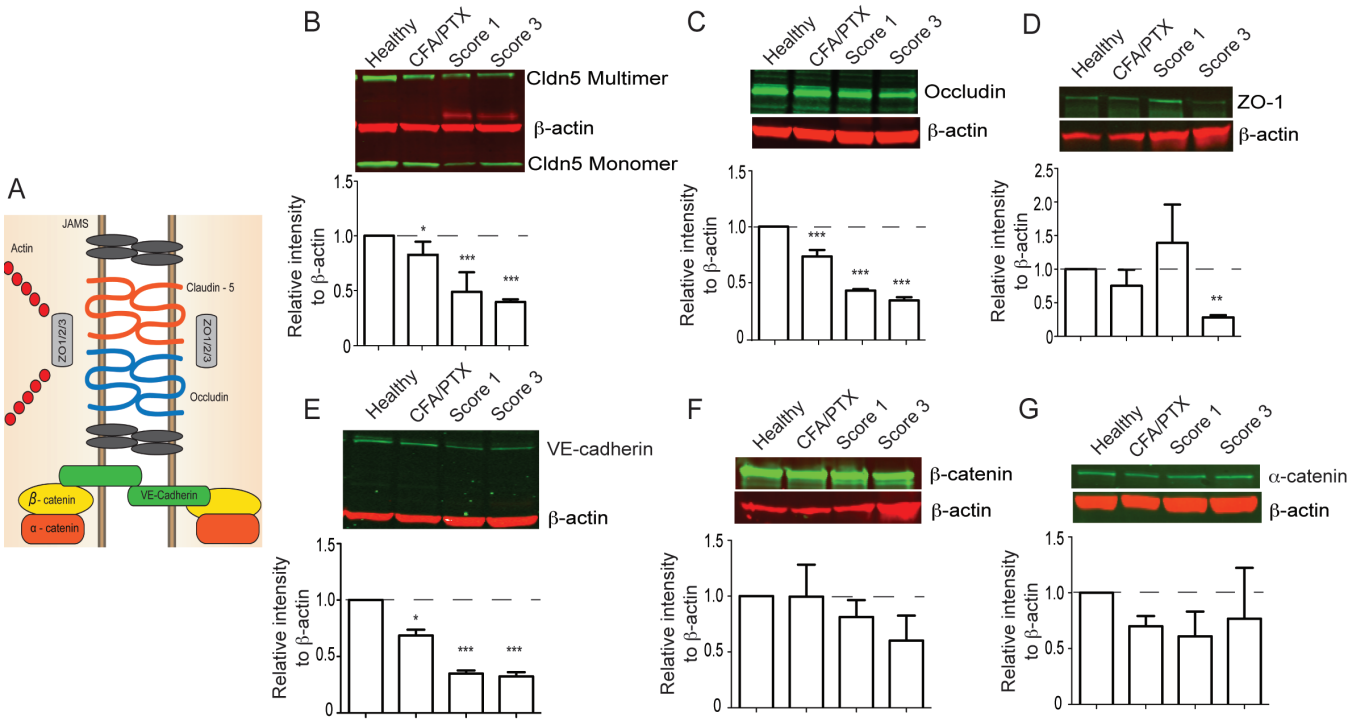

Figure S4. Degradation of adherens and tight junction proteins during EAE progression. A) Schematic diagram of adherens and tight junction proteins expressed in endothelial cells. LICOR fluorescence Western blotting and quantitation for tight junction proteins Claudin-5 (B), Occludin (C) and ZO-1 (D) and adherens junction proteins Cadherin-5 (E), α-catenin (F), and β-catenin (G), from spinal cord lysates in either healthy, CFA/PTX controls or EAE score 1 and 3. β-actin serves as a loading control. Cadherin-5, Claudin-5 and Occludin levels were significantly decreased during EAE progression (n=3 samples per condition, * $p<0.05$, ** $p<0.01$, *** $p<0.001$, one-way ANOVA).

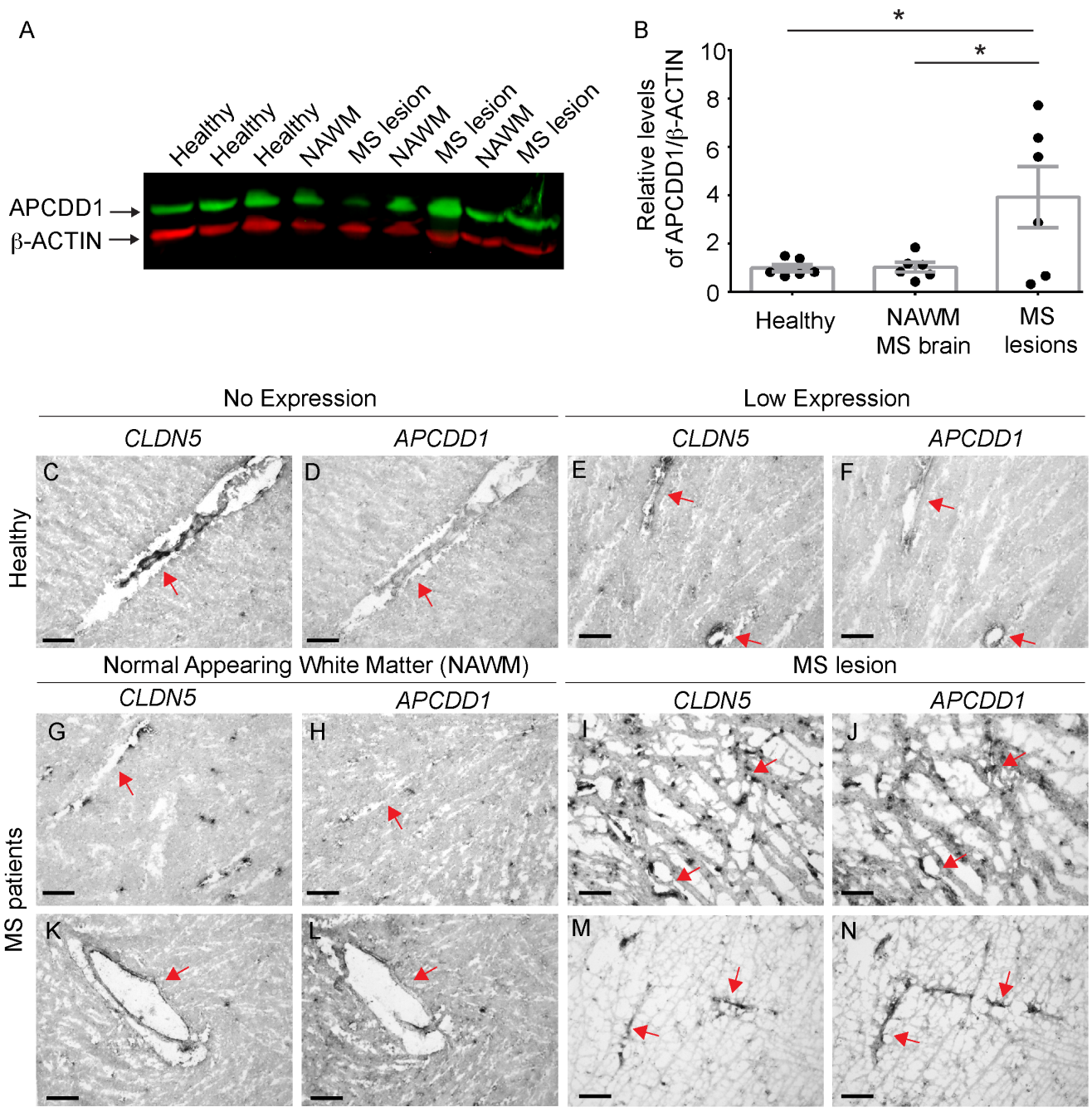

Figure S5. APCDD1 is upregulated in blood vessels from MS lesions. (A, B) LICOR Fluorescence western blotting (A) and quantitation for APCDD1 in lysates from healthy non-MS controls (n=5), normal appearing white matter (NAWM) and lesions of MS patients (n=6). APCDD1 protein levels are increased in lesions in 4 out of 6 MS patients. C-N) Representative images of *in situ* hybridizations for *CLAUDIN5 (CLDN5)* and *APCDD1* in the white matter from healthy non-neurological disease controls

(C-F; n=5; Table 2), NAWM and MS lesions from MS patients (G-N; n=6; Table 2). *APCDD1* mRNA is either absent (D) or low (F) in healthy controls and NAMW in MS patients; however *APCDD1* mRNA levels were higher in MS lesions (I,J,M,N). *APCDD1* mRNA is present in both vascular and non-vascular cells in MS lesions.

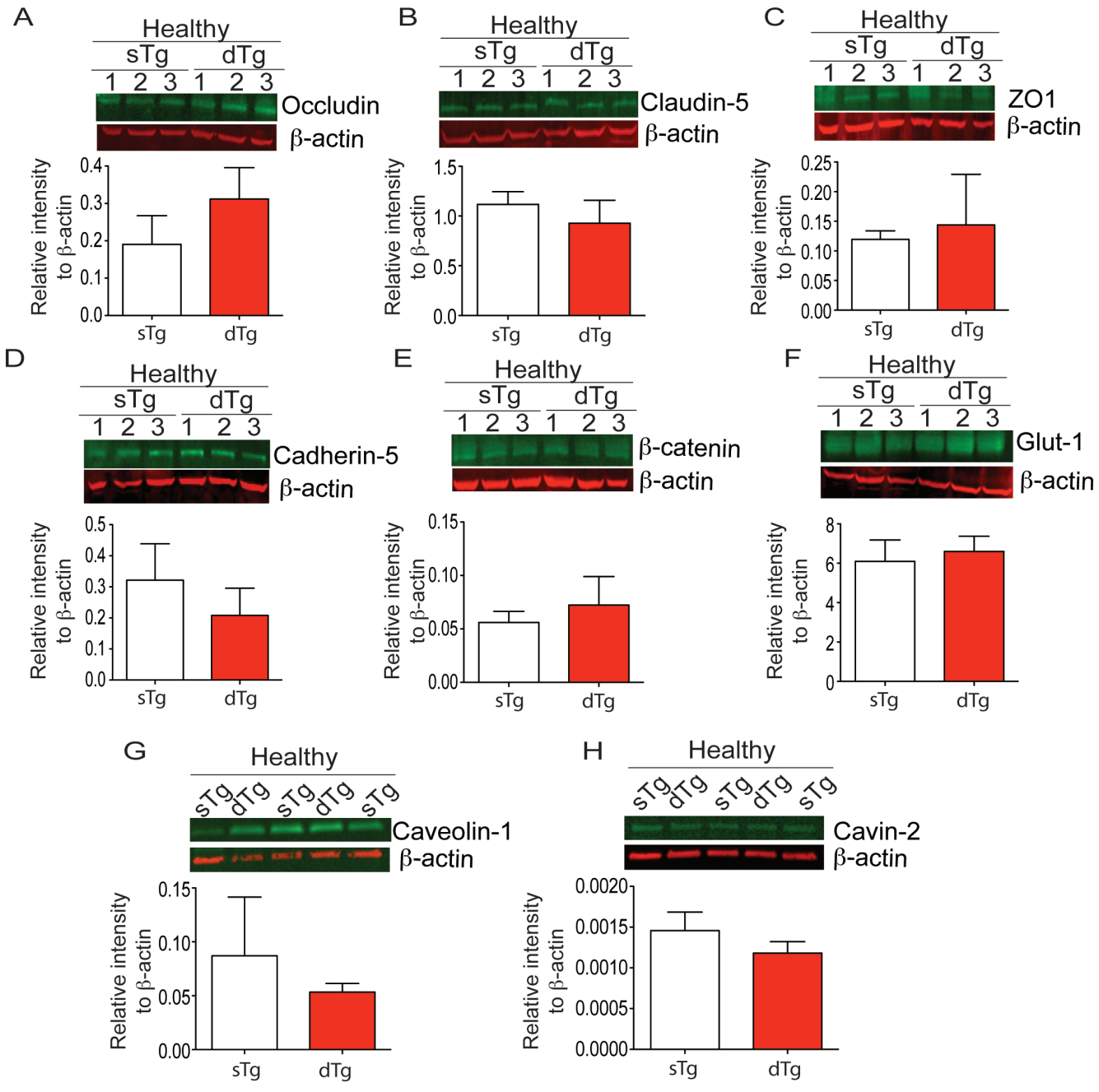

Figure S6. Genetic inhibition of Wnt/β-catenin signaling in CNS ECs by Axin overexpression does not perturb the levels of endothelial adherens and tight junction proteins or transcytosis proteins in healthy mice. LICOR fluorescence Western blotting and quantification for tight junction proteins Occludin (A), Claudin-5 (B) and ZO-1 (C), adherens junction proteins Cadherin-5 (D), β-catenin (E), Glut-1 (F) and caveolar proteins Caveolin-1 (G) and Cavin-2 (H) between sTg and dTg healthy adult mice (60 days after doxycycline removal). β-actin was used as a loading control. All protein levels are not significantly different between sTg and dTg EAE mice (n=3 / group; Student t-test).

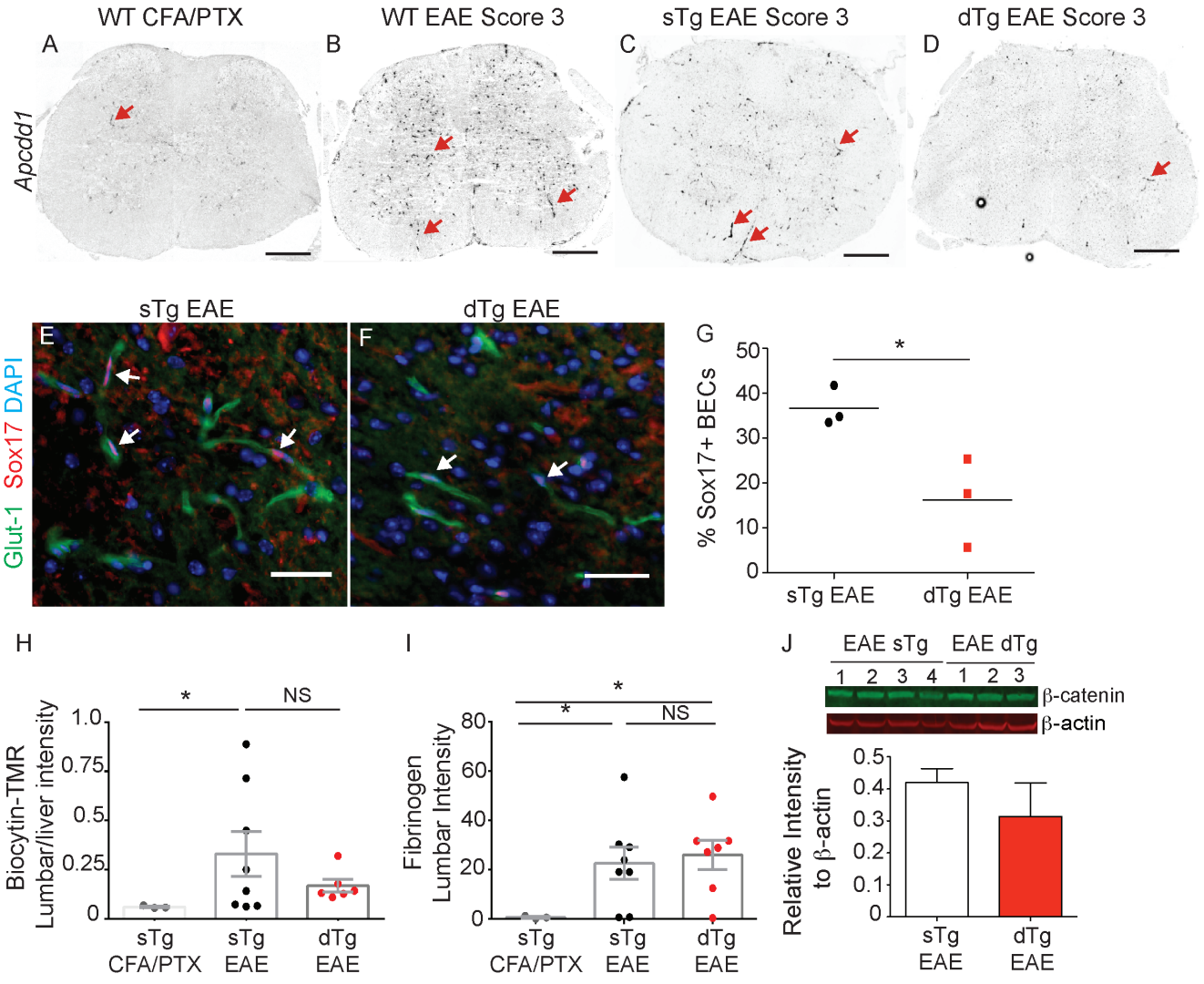

Figure S7. Axin overexpression in ECs inhibits Wnt signaling activation during EAE progression but does not rescue junctional protein degradation or the pathological increase in paracellular BBB permeability. (A-D) In situ hybridization for *Apcdd1 mRNA* in lumbar spinal cords from wild-type CFA/PTX control, wild-type EAE Score 3, sTg and dTg EAE score 3 mice. *Apcdd1* mRNA levels (red arrows) are significantly reduced in dTg, compared to sTg or wild-type EAE mice at similar scores (Score 3). (E-F) Immunofluorescence for Sox17 (red), Glut-1 (blood vessel marker, green) and DAPI (nuclei, blue) in the lumbar spinal cord of sTg and dTg EAE mice of similar scores (Score 3). sTg mice have higher levels of endothelial Sox17 expression (white arrows). G) Dot plots of the fraction of $Sox17^+$ ECs in the lumbar spinal cord of either sTg or dTg EAE mice. There is a significant decrease in the fraction of $Sox17^+$ ECs in dTg EAE mice (n=3 per group, *$p<0.05$; Student t-Test). H) Bar graphs of biocytin-TMR leakage among sTg CFA/PTX controls (n= 3), sTg (n=8) and dTg (n=6) EAE mice. There is no significant difference in biocytin-TMR leakage during EAE between sTg and dTg EAE mice. sTg EAE is significantly greater than sTg CFA/PTX controls (*$p<0.05$; mixed-effect ANOVA). I) Bar graphs of fibrinogen leakage among sTg CFA/PTX controls (n= 3), sTg (n=8) and dTg (n=7) EAE mice. There is no significant difference in fibrinogen leakage during EAE between sTg and dTg EAE mice, but they are both significantly different from sTg CFA/PTX controls (*$p<0.05$; mixed effect ANOVA). Bars represent mean +/- s.e.m. LICOR fluorescence Western blotting and quantitation for β-catenin. β-actin was used as a loading standard. β-catenin is not significantly different between dTg and sTg EAE mice. Scale bars (A-D) are 200 μm and (E-F) are 20 μm.

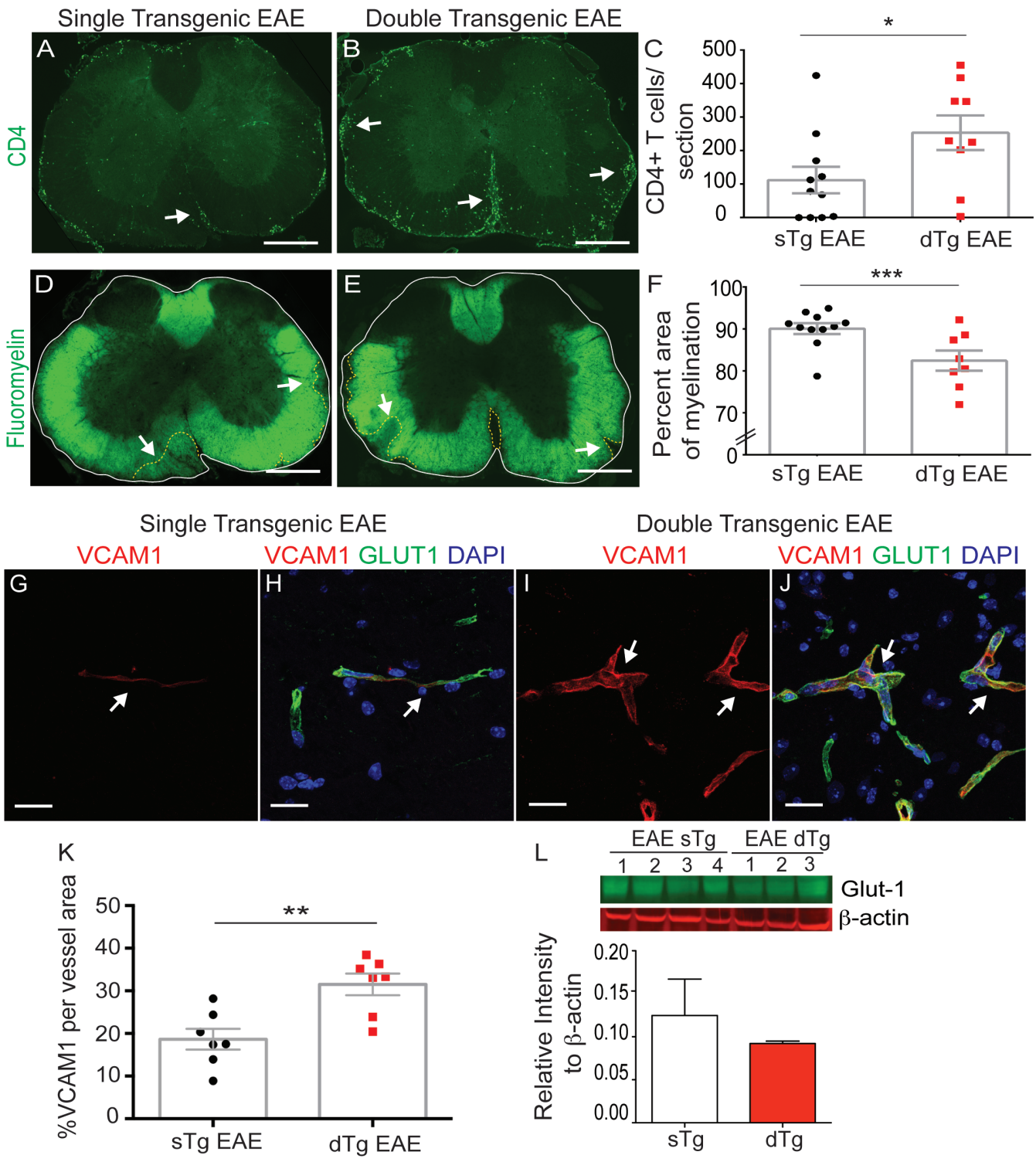

Figure S8. EC-specific inactivation of the Wnt/β-catenin pathway increases immune cell infiltration into the CNS and demyelination by inducing expression of immune cell adhesion molecules in the lumbar spinal cord. A-C) Immunofluorescence and quantitation for $CD4^+$ T cells in

lumbar spinal cords of sTg and dTg EAE mice. White arrows point to $CD4^+$ T cell infiltrates into the CNS. dTg EAE mice have higher $CD4^+$ T-cells within the spinal cord compared to sTg EAE controls (sTg n=11, dTg n=9, *p<0.05; Student t-Test with unequal variance). D-F) Immunofluorescence for myelin (fluoromyelin) and graphs of the fraction of myelinated area in lumbar spinal cords from sTg and dTg EAE mice of similar scores. White arrows point to areas of myelin loss in the white matter lumbar spinal cord. sTg EAE mice have significantly increased myelination compared to dTg EAE mice (sTg n=9, dTg n=7; *p<0.05; Student t-test with unequal variance). G-L) Immunofluorescence for VCAM-1 (red), Glut-1 (blood vessel marker, green) and DAPI (nuclei, blue) in sTg and dTg EAE at lumbar spinal cord. VCAM-1 is highly expressed in blood vessels of dTg EAE mice (I, J, white arrows). K) Quantitation of the fraction of $VCAM\text{-}1^+$ blood vessels in the lumbar spinal cord of sTg and dTg EAE mice. VCAM-1 is significantly elevated in dTg mice during EAE (sTg n=7, dTg n=7, **p<0.01, Student t-Test with unequal variance). L) Fluorescence western blot and quantitation for Glut-1. β-actin serves as a control. Glut-1 expression is not different between sTg and dTg EAE mice (n=4 sTg, n=3 dTg, *p<0.05; Student t-Test with unequal variance). Bar graphs represent mean +/- s.e.m. Scale bars are 200 μm (A, B, D, E) and 20 μm (G-J).

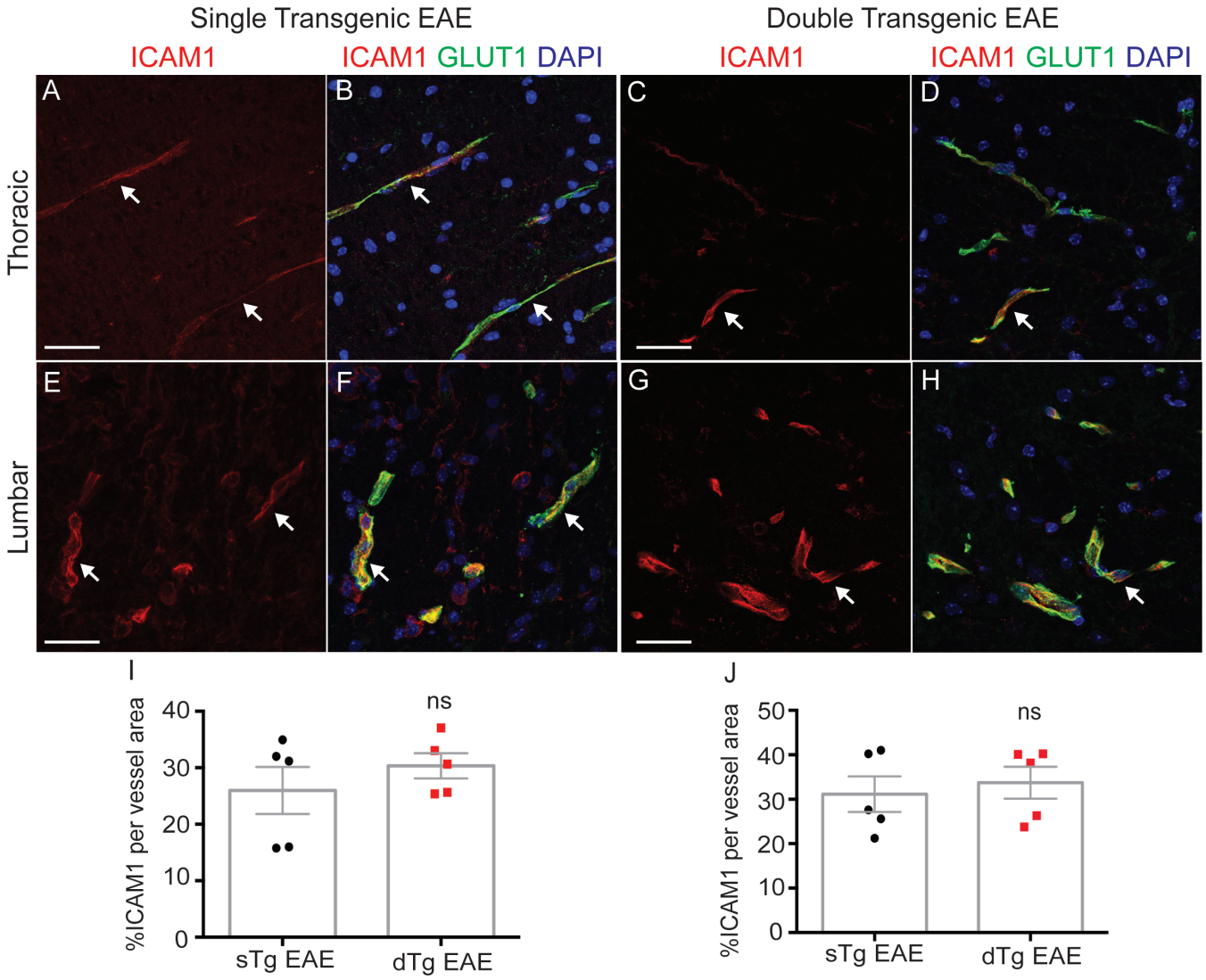

Figure S9. **EC-specific inactivation of the Wnt/β-catenin pathway does not affect expression of ICAM-1 in blood vessels during EAE progression.** A-H) Immunofluorescence for ICAM-1 (red), Glut-1 (blood vessel marker, green) and DAPI (nuclei, blue) in sTg and dTg EAE at both thoracic and lumbar spinal cord. ICAM-1 is equally expressed in blood vessels of both sTg and dTg EAE mice (white arrows). I, J) Quantitation of the fraction of VCAM-1^{+} blood vessels in thoracic and lumbar spinal cord of sTg and dTg EAE mice. ICAM-1 levels are similar between sTg and dTg mice with EAE (sTg n=5, dTg n=5, **p<0.01, Student t-Test with unequal variance). Bar graphs represent mean +/- s.e.m. Scale bars are 20 μm.

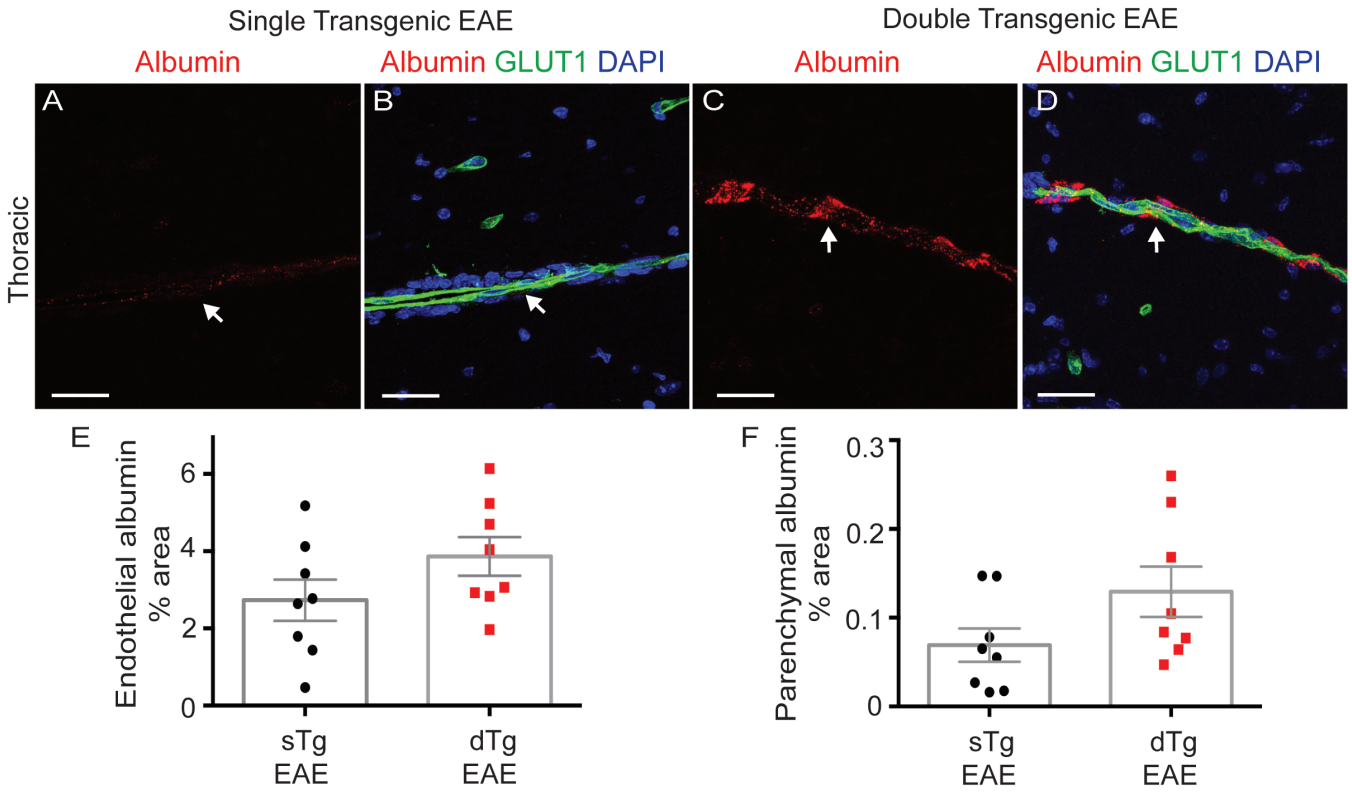

Figure S10. EC-specific inactivation of Wnt signaling pathway increases endothelial cell endocytosis during EAE. A-D) BBB leakage of intravenously injected albumin-Alexa594 (red) in thoracic spinal cord sections from sTg (A,B) and dTg (C,D) mice with EAE at day15 post immunization. The vascular marker Glut-1 (green) labels endothelial cells and DAPI (blue) shows nuclei. E, F) Bar graphs of the fraction of endothelium-associated or parenchyma-associated albumin that has traversed the BBB in the thoracic spinal cord. Each dot represents the mean of multiple fields from a single animal (n = 8 sTg, n= 8 dTg EAE mice). Bar graphs show mean ± SEM. Scale bars are 20 μm.

SUPPLEMENTARY TABLES

Table S1. Expression of Wnt ligands and Norrin in the spinal cord of healthy, CFA/PTX control, and MOG EAE Score 1 and 3 mice.

Probe	Healthy	CFA/PTx	EAE Score 1	EAE Score 3
Wnt-1	+	+	+	+
Wnt-3	+	+	++	+++
Wnt-3a	-	-	-	-
Wnt-4	-	+	+	+
Wnt-5a	+	+	++	++
Wnt-7a	-	-	-	-
Wnt-7b	+	+	+	+
Wnt-9a	-	-	-	-
Wnt-10b	-	-	-	-
Wnt-11	-	-	-	-
Norrin	-	-	-	-

- = no expression

+ = weak expression

++ = intermediate expression

+++ = strong expression

Table S2. Characteristics of patients used in this study

Case	Format	Clinical Diagnosis	Lesions	Age / Sex	Post mortem interval
1	FFPE	MS	Active	31 F	unknown
2	FFPE	MS	Active	50 F	unknown
3	FFPE	MS	Active	39 F	unknown
4	FFPE	MS	Chronic	55 F	unknown
5	FFPE	MS	Chronic	59 F	unknown
6	FFPE	MS	Chronic	69 M	unknown
A	FFPE	MS RR	Chronic	46 F	26H
B	FFPE	MS PP	Active	52 M	18H
C	FFPE	MS RR	Chronic	60 F	21H
D	FFPE	MS SP	Chronic	62 M	4H
E	FFPE	MS	Chronic	64 M	15H
F	FFPE	MS PP	Active	66 F	24H
G	FFPE	Lymphoma	Control	80 M	unknown
H	FFPE	Normal	Control	58 F	7H
I	FFPE	Dementia, etiology not determined	Control	80 M	10H
K	FFPE	Cervical spondylosis	Control	79 F	1H
L	FFPE	Cancer, stomach	Control	61 M	5H
Az	Frozen	MS	Chronic	70 F	16H
Bz	Frozen	MS	Active	81 M	37H
Cz	Frozen	MS	Active	60 M	8H
Dz	Frozen	MS	Active	60 F	15H

Ez	Frozen	MS	Chronic, Active	79 F	25H
Fz	Frozen	MS	Active	63 M	13H
Hz	Frozen	COPD	Control	83 M	20H
Iz	Frozen	Heart attack	Control	68 M	20H
Jz	Frozen	Congestive heart failure	Control	87 M	9H
Kz	Frozen	Cancer, pancreas	Control	73 F	19H
Lz	Frozen	Cancer, pancreas	Control	80 M	19H

Abbreviations:

FFPE: formalin-fixed paraffin embedded

MS multiple sclerosis

MS RR multiple sclerosis relapsing remitting

MS PP multiple sclerosis primary progressive

MS SP multiple sclerosis secondary progressive

COPD Chronic Obstructive Pulmonary Disease

Table S3. Expression of *APCDD1* mRNA in human brain white matter from control and MS cases.

Case	**Clinical diagnosis**	**Normal Appearing White Matter**	**MS lesion**
Az	MS RR	-	+
Bz	MS RR	+	+++
Cz	MS RR	++	+++
Dz	MS RR	-	++

Ez	MS RR	+	+++
Fz	MS RR	-	-
Hz	COPD	-	**N/A**
Iz	Heart attack	++	**N/A**
Jz	Congestive heart failure	+++	**N/A**
Kz	Cancer, pancreas	-	**N/A**
Lz	Cancer, pancreas	++	**N/A**

- = no expression

+ = weak expression

++ = intermediate expression

+++ = strong expression

SUPPLEMETARY REFERENCES

1. Ferrer-Vaquer A*, et al.* (2010) A sensitive and bright single-cell resolution live imaging reporter of Wnt/ss-catenin signaling in the mouse. *BMC Dev Biol* 10:121.
2. Sun JF*, et al.* (2005) Microvascular patterning is controlled by fine-tuning the Akt signal. *Proceedings of the National Academy of Sciences of the United States of America* 102(1):128-133.

3. Hsu W, Shakya R, & Costantini F (2001) Impaired mammary gland and lymphoid development caused by inducible expression of Axin in transgenic mice. *The Journal of cell biology* 155(6):1055-1064.

4. Lutz SE*, et al.* (2013) Contribution of pannexin1 to experimental autoimmune encephalomyelitis. *PloS one* 8(6):e66657.

5. Lutz SE, Raine CS, & Brosnan CF (2012) Loss of astrocyte connexins 43 and 30 does not significantly alter susceptibility or severity of acute experimental autoimmune encephalomyelitis in mice. *Journal of neuroimmunology* 245(1-2):8-14.

6. Frohman EM, Racke MK, & Raine CS (2006) Multiple sclerosis--the plaque and its pathogenesis. *New England Journal of Medicine* 354(9):942-955.

7. Corada M*, et al.* (2013) Sox17 is indispensable for acquisition and maintenance of arterial identity. *Nature communications* 4:2609.

8. Knowland D*, et al.* (2014) Stepwise recruitment of transcellular and paracellular pathways underlies blood-brain barrier breakdown in stroke. . *Neuron* 82:1-15.

9. Shimomura Y*, et al.* (2010) APCDD1 is a novel Wnt inhibitor mutated in hereditary hypotrichosis simplex. *Nature* 464(7291):1043-1047.

10. Daneman R*, et al.* (2009) Wnt/beta-catenin signaling is required for CNS, but not non-CNS, angiogenesis. *Proceedings of the National Academy of Sciences of the United States of America* 106(2):641-646.